

# ***INTEGRAL*, *XMM-Newton* and ESO/NTT identification of AX J1749.1–2733: an obscured and likely-distant Be/X-ray binary<sup>★</sup>**

J.A. Zurita Heras<sup>1</sup> and S. Chaty<sup>1</sup>

Laboratoire AIM, CEA/DSM-CNRS-Université Paris Diderot, DAPNIA/Service d'Astrophysique, Bât. 709, CEA-Saclay, FR-91191 Gif-sur-Yvette, France e-mail: juan-antonio.zurita-heras@cea.fr; sylvain.chaty@cea.fr

Received XXXX; accepted XXXX

## **ABSTRACT**

**Context.** AX J1749.1–2733 is an unclassified transient X-ray source discovered during surveys by *ASCA* in 1993–1999. The transient behaviour and the short and bright flares of the source led to think that it is part of the recently revealed sub-class of supergiant fast X-ray transient.

**Aims.** A multi-wavelength study in NIR, optical, X-rays and hard X-rays of AX J1749.1–2733 is undertaken in order to determine its nature.

**Methods.** Public *INTEGRAL* data and the target of opportunity observation with *XMM-Newton* that we triggered are used to study the high-energy source through timing and spectral analysis. Multi-wavelength observations in optical and NIR with the ESO/NTT telescope are also performed to search for the counterpart.

**Results.** AX J1749.1–2733 is a new high-mass X-ray binary pulsar with an orbital period of  $185.5 \pm 1.1$  days and a spin period of  $\sim 66$  s, typical of a Be/X-ray binary. The outbursts lasts  $\sim 12$  d. A spin down of  $\dot{P} = 0.08 \pm 0.02$  s yr<sup>−1</sup> is also observed, likely due to propeller effect. The most accurate X-ray position is R.A. (2000) = 17<sup>h</sup>49<sup>m</sup>06.8<sup>s</sup> and Dec. = −27°32′32.5″ (uncertainty 2″). The high-energy broad-band spectrum is well fitted with an absorbed powerlaw and a high-energy cutoff with values  $N_H = 20.1^{+1.5}_{-1.3} \times 10^{22}$  cm<sup>−2</sup>,  $\Gamma = 1.0^{+0.1}_{-0.3}$  and  $E_{\text{cut}} = 21^{+5}_{-3}$  keV. A faint Fe K $\alpha$  fluorescence line is also detected at 6.41<sup>+0.08</sup><sub>−0.07</sub> keV and  $EW = 52.5$  eV. The only optical/NIR candidate counterpart within the X-ray error box has magnitudes of  $R = 21.9 \pm 0.1$ ,  $I = 20.92 \pm 0.09$ ,  $J = 17.42 \pm 0.03$ ,  $H = 16.71 \pm 0.02$  and  $K_s = 15.75 \pm 0.07$ , which points towards a Be star located far away ( $> 8.5$  kpc) and highly absorbed ( $N_H \gtrsim 1.7 \times 10^{22}$  cm<sup>−2</sup>). The 22–50 keV luminosity is  $0.4 - 0.9 \times 10^{36}$  ergs s<sup>−1</sup> during the long outbursts with a peak of  $3 \times 10^{36}$  ergs s<sup>−1</sup> during the bright flare occurred at MJD 52891.

**Key words.** X-ray: binaries – X-rays: individual: AX J1749.1–2733 – Infrared: stars

## **1. Introduction**

High-mass X-ray binaries (HMXB) are systems composed of a compact object (either a neutron star (NS) or a black hole (BH)) and a massive companion star. The emission in X-rays is explained by the accretion of the stellar wind coming from the companion and captured by the compact object. There are mainly two classes of HMXB depending on the nature of the massive primary star that has important implications on the X-ray observational features. One might read White et al. (1995) and Psaltis (2006) (and references therein) for large reviews of HMXB.

The first class is composed by a supergiant star (spectral type OB) (later called sgHMXB). In sgHMXB, the compact object orbits within a few days (3–15 d) of the massive companion in circular (or slightly eccentric) orbits. Supergiant stars possess a dense stellar wind that is partly captured by the compact object. This happens either by direct spherical accretion or by Roche-

Lobe overflow via an accretion disk on the compact object. As the compact object always orbits within the stellar wind, these systems are persistent X-ray emitting object and show high variations on short time scales. Moreover, in HMXB with a neutron star, the presence of strong magnetic field modulates the X-ray emission that varies with the spin of the NS. The broad X-ray spectrum is very hard and might display features such as an intrinsic absorption and the presence of the iron fluorescence line at 6.4 keV. Very few of these systems were known before *INTEGRAL*'s launch (Lutovinov et al. 2005; Dean et al. 2005; Bodaghee et al. 2007). The mission allowed the discovery of several new sources that could be identified as sgHMXB (e.g. Walter et al. 2006; Chaty et al. 2008). These sources show typical hard X-ray spectra of accreting pulsars, and most of them show a strong absorption leading to name them as obscured HMXB (e.g. Walter et al. 2003; Filliatre & Chaty 2004; Rodriguez et al. 2006; Bodaghee et al. 2006; Zurita Heras et al. 2006).

The other group is composed of a Be star accompanying the compact object, mostly a NS. A Be star is a fast-rotating B star possessing a dense and slow stellar wind at the equator (thus creating a disk-like ring of matter surrounding the B star). The group of BeHMXB is the most numerous in the HMXB family (Liu et al. 2000, 2006). They possess wide and eccentric orbits ( $P_{\text{orb}} > 15$  days,  $e \gtrsim 0.3$ ). They display either recurrent outbursts near the periastron passage whose duration is normally linked to the orbital period (most common outbursts), or giant

Send offprint requests to: J.A. Zurita Heras

<sup>★</sup> Based on observations with 1) *INTEGRAL*, an ESA project with instruments and science data centre funded by ESA member states (especially the PI countries: Denmark, France, Germany, Italy, Switzerland, Spain), Czech Republic and Poland, and with the participation of Russia and the USA; 2) *XMM-Newton*, an ESA science mission with instruments and contributions directly funded by ESA Member States and NASA; and 3) ESO observations through programme #079.D–0432(A).

outbursts that can last from weeks to months. In most cases, their X-ray emission is modulated by the strong magnetic field of the NS. Otherwise, their spectra are similar to those of supergiants X-ray binaries (see reviews of Bildsten et al. 1997; Coe 2000; Negueruela 2007).

Among the new sources, *INTEGRAL* might have unveiled a new subclass of sgHMXB. Indeed, several newly discovered sources were identified as galactic X-ray sources with a supergiant companion and displaying a transient behaviour (e.g. IGR J17544–2619, in’t Zand 2005; Pellizza et al. 2006). The quiescent level in these systems is of the order of  $10^{32-33}$  ergs s<sup>−1</sup> (e.g. IGR J08408–4503, Götz et al. 2007; Leyder et al. 2007). The X-ray luminosity increases up to  $10^{36}$  ergs s<sup>−1</sup> (as observed in the known sgHMXB) only during short luminous-flares activity. The X-ray luminosity remains at a very low level (if not totally absent) during most of the time, except during the flares. These flaring periods last for a few hours at most and then the source goes back to an undetectable level of emission (e.g. XTE J1739–302, Smith et al. 2006). Therefore, they received the name of Supergiant Fast X-ray Transient (SFXT) (Negueruela et al. 2006). Except the transient nature of SFXT, their spectral features are similar to the previously known persistent sgHMXB.

The unclassified transient X-ray source AX J1749.1–2733 was discovered at a very low-luminosity level during the ASCA galactic centre survey performed between 1993 and 1999 (Sakano et al. 2002). Its position is R.A. (2000) = 17<sup>h</sup>49<sup>m</sup>09.0<sup>s</sup> and Dec. = −27°33′13.9″ (50″ at 90% confidence). The source was detected three times over the six observations where the source was located within the instruments field of view. The observed 0.7–10 keV flux varies between  $(2 - 6) \times 10^{-12}$  ergs cm<sup>−2</sup> s<sup>−1</sup>. Each spectrum is fitted with an absorbed power law model. However, only in one observation are the parameters well constrained with  $\Gamma = 2.1^{+4.7}_{-2.6}$  and  $N_H = 25^{+57}_{-21} \times 10^{22}$  cm<sup>−2</sup>.

A new flare of this source has been observed by *INTEGRAL* on Sept. 9, 2003, lasting 1.3 days (Sguera et al. 2006). The 20–60 keV peak flux was 40 mCrab and they fitted the spectrum with a combination of a black body and a power law ( $KT = 0.7^{+0.3}_{-0.1}$  keV and  $\Gamma = 2.5 \pm 0.2$ ). Due to the shortness of the flare, they classified this source as a candidate SFXT. This tentative classification was already pointed out by in’t Zand (2005) and references therein. Kuulkers et al. (2007) also report *INTEGRAL* detections in the periods Feb.–Apr. in 2005 and 2006, and non-detection in 2005 Aug.–Oct. The average 20–60 keV flux is rather low with < 2 mCrab in both detections<sup>1</sup>.

Furthermore, analyzing all *INTEGRAL* public data, we discovered a likely-period of ∼ 185 days that we reported in Zurita Heras et al. (2007) as an advance of this work. The source is detected by *INTEGRAL* at a level of  $\geq 5\sigma$  for a few days during March and September each year. In our ATel, we strengthened our discovery reporting more recent *INTEGRAL* detections thanks to the data available in the public page of the *INTEGRAL* Galactic Bulge program<sup>1</sup>. These detections agree with the ∼ 185 d period. Therefore, following our announcement, we asked for a target of opportunity (ToO) observation with *XMM-Newton* during the expected outburst of March 2007 which was accepted.

Following this announcement, *Swift* performed a ToO observation of 5 ks on March 30, 2007 (Romano et al. 2007)<sup>2</sup>.

They detected a bright source at the position R.A. (2000) = 17<sup>h</sup>49<sup>m</sup>06.8<sup>s</sup> and Dec. = −27°32′30.6″ (6.3″ at 90% confidence), 31″ away from the ASCA position. Still, the ASCA position reported in the ATel does not correspond to the one published in Sakano et al. (2002) with a shift of 20″, so the real separation is 51″. Its spectrum could be fitted with an absorbed power law ( $N_H = 23^{+14}_{-10} \times 10^{22}$  cm<sup>−2</sup>,  $\Gamma = 2.5^{+2.0}_{-1.7}$ ) and the observed 2–10 keV flux is  $\sim 10^{-11}$  ergs cm<sup>−2</sup> s<sup>−1</sup>. The *Swift*/UVOT telescope did not detect any optical counterpart with a  $3\sigma$  upper limit of  $V = 20.67$  mag. Within the error box, Romano et al. (2007) reports three 2MASS candidate counterparts whose infrared (IR) magnitudes in the JHK bands suggest a strong optical extinction of 20 mag. One candidate is compatible with a supergiant and the two others are more likely B stars. Thus, the nature of AX J1749.1–2733 remains a mystery.

From the *XMM-Newton* observation, Karasev et al. (2007) reported the discovery of a pulsation of ∼ 132.1 s. The pulse profile displays a double peak structure with a pulse fraction of ∼ 30% in the 2–10 keV energy range. They also detected a pulsation during the outburst detected by *INTEGRAL* on Sept. 8–10, 2003 in the 20–60 keV energy range with a higher pulse fraction of 50%.

Here we report multiwavelength observations performed on AX J1749.1–2733 with *INTEGRAL*, *XMM-Newton* and the ESO/NTT telescope. In Sect. 2, we first describe the observations and the data analysis of each instrument. Then, we present the results in Sect. 3. Finally, we finish with a discussion and the conclusion on the nature of the source in Sect. 4.

## 2. Observations and data analysis

The present work is based on data of two spatial high-energy missions, *INTEGRAL* (Winkler et al. 2003) and *XMM-Newton* (Jansen et al. 2001), of the European Space Agency (ESA). Multi-wavelength follow-up observations were also performed with the ESO<sup>3</sup> 3.5 m New Technology Telescope (NTT) at La Silla Observatory, Chile.

### 2.1. INTEGRAL

The INTERNATIONAL Gamma-Ray Astrophysics Laboratory (*INTEGRAL*) is a hard X-ray and  $\gamma$ -ray spacecraft (S/C) laboratory operating since October 2002. The scientific payload is composed of four instruments. However, only data from the hard X-ray and soft  $\gamma$ -ray coded-mask imager IBIS/ISGRI (15–300 keV) (Ubertini et al. 2003; Lebrun et al. 2003) are going to be considered in this work. The imager possesses a large field of view (FOV) of 29° square with a spatial resolution of 12′.

The source is located near the galactic centre at a distance of 1.6°. As the galactic centre is one of the major scientific goal of *INTEGRAL*, the source’s field has been largely observed. All public data available on march 2007 for AX J1749.1–2733 have been considered in this work. Only pointings where the source is located less than 14° from the FOV centre and whose time exposure is larger than 600 s are kept. In total, it represents 4759 pointings distributed in 129 revolutions of the S/C that goes from Feb., 2003 (revolution 46, MJD 52698.0) to Oct., 2005 (revolution 370, MJD 53670.1). The total exposure time on the source

<sup>1</sup> see the public page of the *INTEGRAL* Galactic Bulge program at <http://isdc.unige.ch/Science/BULGE> for further informations.

<sup>2</sup> From the same observation, Kong (2007) also reports a slightly more accurate position with R.A. (2000) = 17<sup>h</sup>49<sup>m</sup>06.8<sup>s</sup> and Dec. =

−27°32′31.5″ (3.8″ at 90% confidence). He also fitted the spectrum with an absorbed power law with  $N_H = (19 \pm 9) \times 10^{22}$  cm<sup>−2</sup>,  $\Gamma = 2.1 \pm 1.2$  and an absorbed 2–10 keV flux of  $\sim 6 \times 10^{-12}$  ergs cm<sup>−2</sup> s<sup>−1</sup>.

<sup>3</sup> European Southern Observatory

is 10.8 Ms (*i.e.* 125.4 days) spanned over the 2.5 years of observations. They are not equally distributed along this period due to scheduling reason.

The ISGRI data are reduced using the Offline Scientific Analysis (OSA<sup>4</sup>) version 6.0 software that is publicly released by the *INTEGRAL* Science Data Centre (ISDC) (Courvoisier et al. 2003). Individual sky images for each pointing have been produced in the energy band 22–50 keV. Sky mosaics with longer exposures have been built combining pointings in which the source is not detected at a  $5.1\sigma$  level or higher in individual pointings. The light curves are built using the imaging products. The source count rate is extracted with help of the tool *mosaic\_spec* (version 1.4) that is part of the OSA package. Detection of the source in mosaics are considered at a  $6\sigma$  level or higher. We extract a spectrum of the source during the first bright flare detected with ISGRI. The spectral extraction was performed using the recently released OSA version 7.0. The source spectrum is extracted with *ii\_spectra\_extract* within OSA for each pointing. Then, each individual spectra are summed to build one single spectrum of the source using the OSA tool *spe\_pick*. The redistribution matrix file (RMF) *isgr\_rmf\_grp\_0025.fits* is rebinned into 5 channels spread between 15 and 80 keV. Light curves with a binning of 10 s of the first bright flare observed with ISGRI are also extracted with *ii\_light* version 8.2. The light curves are given in counts s<sup>-1</sup>. The 22–50 keV count rates are converted into other units with the relation 1 Crab = 117 counts s<sup>-1</sup> =  $9 \times 10^{-9}$  ergs cm<sup>-2</sup> s<sup>-1</sup>. The time unit IJD corresponds to MJD = IJD + 51544.

## 2.2. XMM-Newton

The main scientific instrument on-board the X-ray Multi-Mirror Mission (*XMM-Newton*) satellite is the EPIC camera composed of two MOS (Turner et al. 2001) and one pn (Strüder et al. 2001) CCD cameras. It has imaging, timing, and spectral capabilities in the 0.2–12 keV energy range with a 30' FOV. The EPIC cameras were operating in imaging science mode with full window for MOS1, large window for MOS2 and pn and with medium filters for each camera.

AX J1749.1–2733 was observed with *XMM-Newton* on March 31, 2007, from 08:03:37 to 11:27:40 UTC (MJD 54190.337–54190.478) for a total exposure of 12.2 ks. There is no simultaneous observation with *INTEGRAL*.

Events lists for each MOS and pn cameras are generated with the Science Analysis Software (SAS<sup>5</sup>) version 7.0.0 using the *emproc* and *epproc* tool, respectively. The event lists are corrected for enhanced background features observed at energies higher than 10 keV, disregarding time lapses when count rates exceed 0.52 counts s<sup>-1</sup> for pn and 0.2 counts s<sup>-1</sup> for both MOS. Therefore, the net exposure is 5.6 out of 10 ks exposure for pn, 10.8 out of 12 ks for MOS1 and 11.1 out of 12 ks for MOS2. Images for MOS[12] and pn are generated with 2'' and 4'' resolution, respectively, using good events until the quadruple level in the 0.8–10 keV energy range and disregarding bad pixels. An accurate X-ray position determined with EPIC is calculated with the SAS task *edetect\_chain*. Four images with energy ranges 0.5–2, 2–4.5, 4.5–7.5, and 7.5–12 keV for each MOS and pn cameras are extracted. Then, the best position for each individual EPIC camera is determined. Finally, the best source position is calculated as the mean of the positions given by the three cam-

eras. The source location precision is limited by the astrometry of the S/C that is of 2''<sup>6</sup>, the statistical error of 0.1'' being insignificant in comparison.

In the EPIC/pn image, one bright source is detected in the CCD#1 near the read-out node. The event list of the source+background is extracted from a region of 35'' radius centered on the source. A background event list is extracted in the same CCD at same distance of the read-out node from a region of similar size not affected by the bright source. Spectra are extracted selecting single+double events but disregarding bad pixels. Specific RMF and ancillary response files (ARF) are generated with the SAS tasks *rmfgen* and *arfgen*, respectively. The Xspec version 11.3.2t package (Arnaud 1996) is used to plot and fit the resulting spectra corrected from background. For light curves, single and double events are also selected within the same regions defined in the spectral step. The source light curves are corrected from the background using the SAS task *lccorr* and we applied the barycentric correction with the SAS task *barycen*.

## 2.3. ESO/NTT

Multiwavelength observations were undertaken soon after the accurate X-ray position was given by Romano et al. (2007) and Kong (2007). The observations were achieved with the 3.5 m ESO/NTT telescope in two domains: in the near IR (NIR) domain (1–2.4  $\mu$ m) with the spectro-imager SOFI and in the optical domain with the imager SUSI-2 (350–900 nm). The observations were carried out as part of the program 079.D-0432(A) (PI: S. Chaty), through service mode. Astrometry, photometry and spectroscopy were achieved during those observations. The spectroscopy was attempted on the likely-supergiant counterpart proposed by Romano et al. (2007) (2MASS source 1).

### 2.3.1. NIR observations

NIR photometry in the bands *J*, *H* and *K<sub>s</sub>* was performed on April 3, 2006, with the spectro-imager SOFI installed on a Nasmyth focus of the NTT. The observations were centered on the known X-ray position of AX J1749.1–2733. The large imaging mode was used during those observations that gives an image pixel scale of 0.288'' and a FOV of 4.92'  $\times$  4.92'. Nine images were taken for each band with integration times of 60 s for *J* and 47.3 s for *H* and *K<sub>s</sub>*. For each band, four of the nine observations were taken with a slight offset of  $\sim 30''$  that allow us to build the NIR sky in order to subtract it from the images. Six standard stars chosen in the faint NIR standard stars catalogue (Persson et al. 1998) were also observed: S262-E, S495-E, S708-D, S264-D, P565-C and S875-C. Five observations per band were performed on each standard stars. The first observation was centered on the target and then, the next four images were taken with an offset of  $\sim 45''$  compared to the first one.

### 2.3.2. Optical observations

The optical observations were carried out on April 6, 2007, between UTC 08h40 and 08h40 with the imager SUSI-2 also installed on the same Nasmyth focus of the NTT as SOFI. Optical photometry in *U*, *B*, *V*, *R*, *I* and *Z* bands was obtained. The FOV is of 5.5'  $\times$  5.5' with a binning of factor 2 that gives a pixel scale of 0.161'' per pixel. The exposure time is 60 s for each

<sup>4</sup> OSA is available at <http://isdc.unige.ch/?Soft+download>

<sup>5</sup> SAS is available at [http://xmm.vilspa.esa.es/external/xmm\\_sw\\_cal/sas.shtml](http://xmm.vilspa.esa.es/external/xmm_sw_cal/sas.shtml)

<sup>6</sup> The *XMM-Newton* astrometric accuracy is described in the calibration document XMM-CAL-TN-0018.

filter. 9 photometric standards (selected in the optical standard star catalog of Landolt 1992) were also observed in the fields PG 1657+078 and PG 1633+099. The integration times in each filter vary between 10–100 s.

### 2.3.3. Data reduction

The reduction of both optical and NIR data is performed with the Image Reduction and Analysis Facility (IRAF<sup>7</sup>) version 2.13beta2. Data reduction was performed using standard procedures on the optical and NIR images, including the correction of the dark current, the flat-fielding and NIR sky subtraction.

We performed accurate astrometry on each image ( $U, B, V, R, I, Z, J, H, K_s$ ) using the *gaia* tool from the Starlink suite<sup>8</sup> and using the 2MASS catalogue for the NIR images and the USNO B1.0 catalogue for the optical images. The NIR rms of astrometry fit is always lower than  $0.4''$  with the expected pixel scale in x,y axis of  $-0.288 \times 0.288''/\text{pixel}$ . The optical rms of astrometry fit is also lower than  $0.4''$  with the expected pixel scale in x,y axis of  $0.161 \times 0.161''/\text{pixel}$ .

Then, we carried out aperture photometry in a crowded field using the IRAF *digiphot.daophot* package. The instrumental magnitudes  $m_{\text{instr}}$  are transformed into apparent magnitudes  $m_{\text{app}}$  using the standard photometric relation:  $m_{\text{app}} = m_{\text{instr}} - Z_p - ext \times AM$ , where  $Z_p$  is the zero-point,  $ext$  the extinction and  $AM$  the airmass. The colour term is not used because 1) there are not enough standard stars in NIR and 2) in optical bands, we do not detect the sources of interest in several bands (particularly in V) in order to perform colour correction. The  $Z_p$  and  $ext$  parameters are fitted using the photometric relation in order to match the instrumental and apparent magnitudes of the standard stars. For the optical photometry, the extinction parameters are fixed to the values given during the SUSI-2 calibration<sup>9</sup>. The airmass, zero-point and extinction parameters are reported at the bottom of Table 4.

## 3. Results

### 3.1. Refined X-ray position

A 22–50 keV image has been generated from the first outburst whose pointings are listed in Table 1. The source is detected at a level of  $44\sigma$  for a total exposure of 51.3 ks (see Fig. 1). The best hard X-ray position is R.A. (2000) =  $17^{\text{h}}49^{\text{m}}05.5^{\text{s}}$  and Dec. =  $-27^{\circ}32'38.4''$  with an error of  $1.8'$  related to its significance (Gros et al. 2003). This position is consistent with the position previously reported in the 3rd ISGRI catalogue (Bird et al. 2006) and in Sguera et al. (2006).

One bright source lies within the AX J1749.1–2733 ISGRI error box in EPIC images (see Fig. 2). The best position determined with EPIC is R.A. (2000) =  $17^{\text{h}}49^{\text{m}}06.8^{\text{s}}$  and Dec. =  $-27^{\circ}32'32.5''$  with a systematic uncertainty of  $2''$ . This X-ray refined position is consistent with the respective error boxes of *ASCA*, *INTEGRAL* and *Swift*. There is only a difference of  $1''$  between the *Swift* and the EPIC positions.

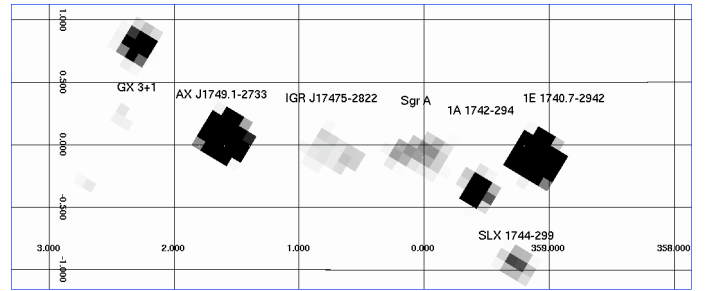


**Fig. 1.** ISGRI 22–50 keV significance map built with the pointings of rev. 110 listed in Table 1 corresponding to the first outburst of AX J1749.1–2733 observed with *INTEGRAL*. AX J1749.1–2733 is located near the galactic centre and it is detected with a significance of  $44\sigma$  for an exposure of 51.3 ks. The coordinate grid corresponds to the galactic longitude and latitude  $l, b$  in degrees.

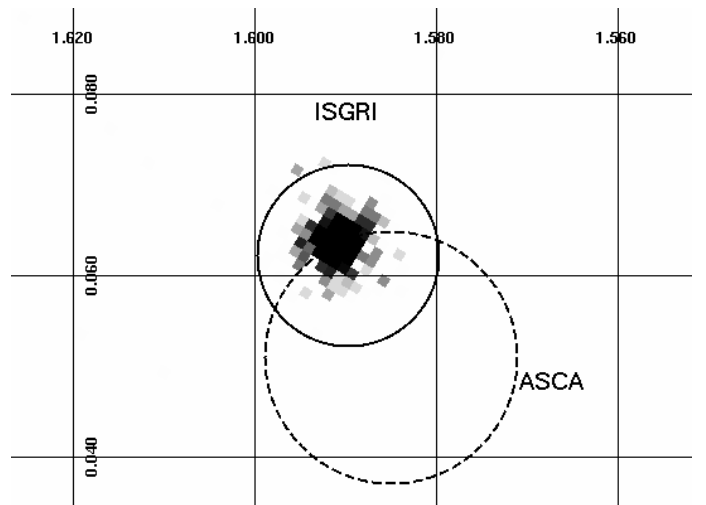


**Fig. 2.** EPIC/MOS1 image in the 0.8–10 keV energy range. The ISGRI (derived from the 1st outburst) and ASCA error boxes are reported, the *Swift* position being well embedded in the bright source. The best EPIC position is R.A. (2000) =  $17^{\text{h}}49^{\text{m}}06.8^{\text{s}}$  and Dec. =  $-27^{\circ}32'32.5''$  with a systematic uncertainty of  $2''$  (e.g. galactic  $l, b = 1.5908^{\circ}, 0.0637^{\circ}$ ). The coordinate grid corresponds to the galactic longitude and latitude  $l, b$  in degrees.

### 3.2. Timing analysis

While the long-term variability of AX J1749.1–2733 can be studied with the huge amount of data collected with *INTEGRAL*, *XMM-Newton* allows to study the source on the short-term variability.

#### 3.2.1. Long-term variability

The long-term variability of AX J1749.1–2733 is studied using the ISGRI data in the energy range 22–50 keV. The work is divided in three parts as the source is transient.

First, all detections within one pointing of the S/C indicating an increase of the hard X-ray emission on a short time-scale ( $\lesssim 1$  h) are searched. In total, the source is detected at a level higher than  $5.1\sigma$  in 16 pointings over the 4759 ones (see Table. 1). Two bright outbursts are observed along the 2.5 yr observations, one lasting  $\lesssim 1$  day in revolution 110 (see Fig. 3) (the one reported in Sguera et al. 2006) and another short one in revolution

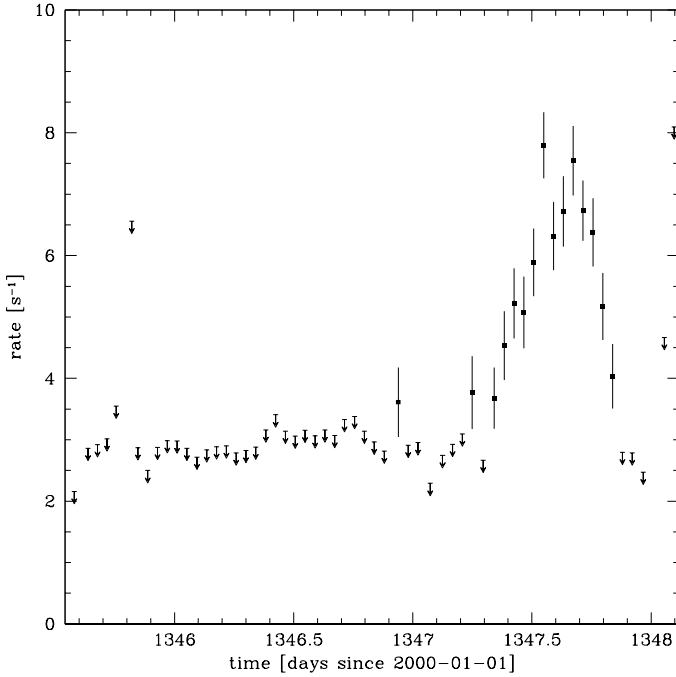
<sup>7</sup> IRAF is available at <http://iraf.net/>

<sup>8</sup> Thanks to the Joint Astronomy Centre, the Starlink software collection is still available at <http://starlink.jach.hawaii.edu/>.

<sup>9</sup> retrieved at <http://www.ls.eso.org/lasilla/sciops/ntt/susi/archive/susi2zp.dat>

**Table 1.** List of detections of AX J1749.1–2733 in single pointings with IBIS/ISGRI. The total exposure of each individual pointing is  $\sim 3.5$  ks. The source displays 2 bright flares, one as long as 0.5 d, one short with  $\sim 3.5$  ks.

Time IJD	22–50 keV Flux counts s <sup>-1</sup>	Error flux counts s <sup>-1</sup>	Sigma	Off-axis angle degrees	Pointing
1346.9390	3.6	0.6	6.4	3.7	01100038
1347.2492	3.8	0.6	6.3	4.7	01100045
1347.3421	3.7	0.5	7.4	0.8	01100047
1347.3836	4.5	0.6	8.1	1.5	01100048
1347.4250	5.2	0.6	9.2	3.4	01100049
1347.4664	5.1	0.6	8.7	4.2	01100050
1347.5078	5.9	0.6	10.7	2.9	01100051
1347.5491	7.8	0.5	14.5	2.6	01100052
1347.5903	6.3	0.6	11.4	3.7	01100053
1347.6318	6.7	0.6	11.7	5.3	01100054
1347.6732	7.5	0.6	13.3	2.7	01100055
1347.7146	6.7	0.5	13.7	0.8	01100056
1347.7560	6.4	0.6	11.5	1.5	01100057
1347.7972	5.2	0.5	9.5	2.0	01100058
1347.8385	4.0	0.5	7.7	1.6	01100059
1534.6049	3.3	0.6	5.5	4.9	01730024

**Fig. 3.** ISGRI 22–50 keV lightcurve of AX J1749.1–2733 during rev. 110.  $5.1\sigma$  upper limits are reported when the source is not detected.

173 lasting 1 h. The source is detected in a few single pointings at a level slightly higher than the detection threshold before displaying a bright outburst that starts at MJD 52891.3636 (*i.e.* IJD 1347.3636) and lasts  $\sim 0.5$  days. The increase/decrease are rather smooth. The peak intensity is reached in the middle of the outburst with two local maxima at  $7.5 - 7.8 \pm 0.5$  counts s<sup>-1</sup> and a small decay in between. The two outbursts are reported in the long-term lightcurve (see Fig. 4).

The non-flaring behaviour of AX J1749.1–2733 is then studied. Detections on larger time-scale are searched. The long-term monitoring of AX J1749.1–2733 is summarized in Table 2. First, the two revolutions in which at least one flare occurred are considered (*i.e.* 110 and 173). We built a mosaic for each revolution where all the pointings without detections are used. The expo-

surements are large with 127 and 144 ks, respectively. In each case, the source is significantly detected with  $11\sigma$  and a faint count rate of  $1.0 \pm 0.1$  (triangle points in Fig. 4). Then, individual mosaics for each revolution are built. The source is again detected in 10 revolutions at a significant level of  $> 6\sigma$  for exposure times between 100–200 ks (square points in Fig. 4). All the detection are distributed in 5 detection periods that are separated by half a year each time. There are 2 isolated revolutions and three periods where the source is detected in consecutive revolutions (3 or more) giving elapsed time of activity of 11.6, 2.5, 2.3, 8.4 and 8.3 days, respectively. However, the observed flux level during the outbursts is faint with rates of  $(0.56 - 1.25) \pm 0.1$ . With such faintness, the exposure time in individual revolution needs to be higher than  $\sim 100$  ks in order to detect the source as we note in Table 2. For each observed outburst except the first one, the revolutions prior and/or after the outburst does not fill this condition. Considering the nearest revolutions having exposure time higher than 100 ks that surround the outbursts, the maximum outburst duration that we derive is  $\leq 18$  d. Only the first outburst duration can be constrained to less than 12.4 d that is the difference between the ending and starting of rev. 109 and 114. Both revolution exposure times are  $\sim 200$  ks, so it firmly exclude any activity of AX J1749.1–2733 with the same level displayed in other detections. The outbursts 1, 4, 5 display similar behaviour with a first detection  $\geq 1$  counts s<sup>-1</sup> followed by fainter detections. Considering the start of this 3 outbursts, we derive a period of  $185.5 \pm 1.1$  d. This period is consistent with the 2 other short detections and the gap or lack of sensitivity. The source is not detected during the first part of the observation as the expected outburst time falls in the middle of a gap of 12 d without observation.

The remaining revolutions are cumulated together only when they are separated by less than 30 days. This results in 11 mosaics with exposures times lying between 333–1005 ks. The  $1\sigma$  level lies between  $0.04$ – $0.07$  counts s<sup>-1</sup> ( $=0.05$ – $0.08$  mCrab). As the field is noisier with exposure times  $> 300$  ks, the detection limit is set to  $10\sigma$  (*i.e.*  $\geq 0.5$  mCrab). The fluxes extracted in these mosaics are also reported in Table 2 (upper limit arrows in Fig. 4). The source is never detected besides the 5 outbursts discussed earlier. The detailed 22–50 keV lightcurve is shown in Fig. 4.

**Table 2.** Long-term monitoring of AX J1749.1–2733 with *INTEGRAL*/IBIS/ISGRI. Detections in individual revolution are reported at the top and then the countrates extracted in large mosaics of consecutive revolutions at the bottom. The last column represents either the revolution number (*top*) or the observed fraction derived as exposure/(time stop–time start) (*bottom*).

Time start IJD	Time stop IJD	22–50 keV Flux counts s <sup>−1</sup>	Flux error counts s <sup>−1</sup>	Detection sigma	Exposure s	revolution or observed fraction
<i>one revolution</i>						
1345.5410	1348.1174	1.08	0.10	11.4	126803	110
1348.6103	1351.1086	0.61	0.08	7.8	176622	111
1351.5239	1354.1001	0.56	0.07	7.8	203381	112
1354.5150	1357.0919	0.61	0.07	8.3	195763	113
1534.1522	1536.6650	0.99	0.09	10.8	143943	173
1722.5068	1724.7996	0.85	0.10	8.8	147812	236
1902.1512	1904.5188	1.08	0.12	9.2	137347	296
1904.9797	1907.4973	0.97	0.08	11.9	192511	297
1907.9482	1910.5226	0.73	0.09	8.6	177189	298
2087.5924	2089.8853	1.25	0.15	8.6	101696	358
2090.6097	2092.9742	0.88	0.11	8.0	129327	359
2093.5752	2095.9587	0.93	0.14	6.5	108779	360
<i>multi-revolutions</i>						
1154.1922	1214.5034	0.34	0.04	7.9	887100	0.17
1324.9592	1345.1323	0.21	0.04	6.0	1004817	0.17
1357.5105	1383.3782	0.26	0.04	6.6	904838	0.40
1507.4945	1530.5140	0.31	0.05	7.0	687994	0.35
1537.7486	1571.5313	0.35	0.04	7.8	668850	0.23
1690.1832	1722.0688	0.36	0.05	7.0	603794	0.22
1725.8560	1762.0251	0.26	0.04	6.8	976316	0.31
1873.1647	1900.9215	0.37	0.07	5.8	333370	0.14
1910.9388	1944.1377	0.37	0.04	8.8	770675	0.27
2055.1532	2086.8640	0.42	0.07	6.2	389952	0.14
2097.9383	2125.8160	0.47	0.05	9.1	658682	0.27

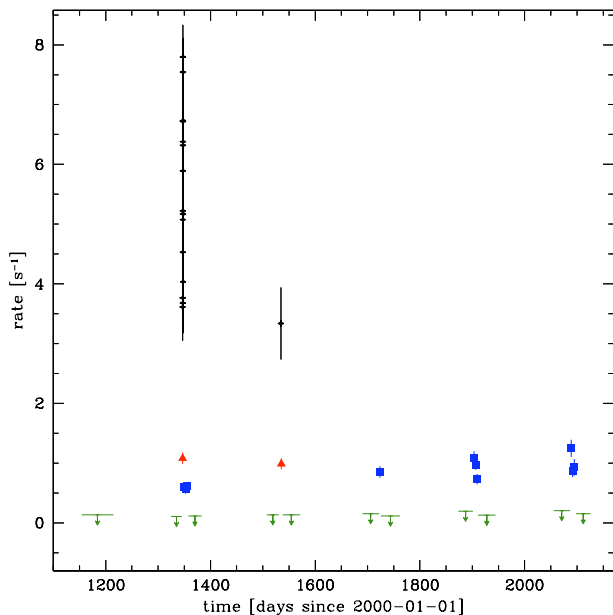


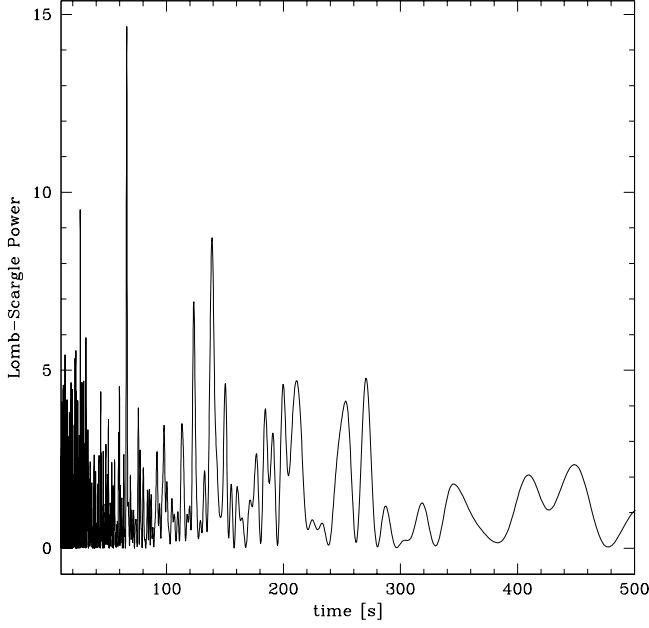
**Fig. 4.** ISGRI 22–50 keV long-term lightcurve of AX J1749.1–2733. The 2 flares reported in Table 1 are shown as vertical crosses for each single pointing. The other points correspond to average count rates extracted in large mosaic images. Details about symbols are found in the text.

### 3.2.2. Short-term variability

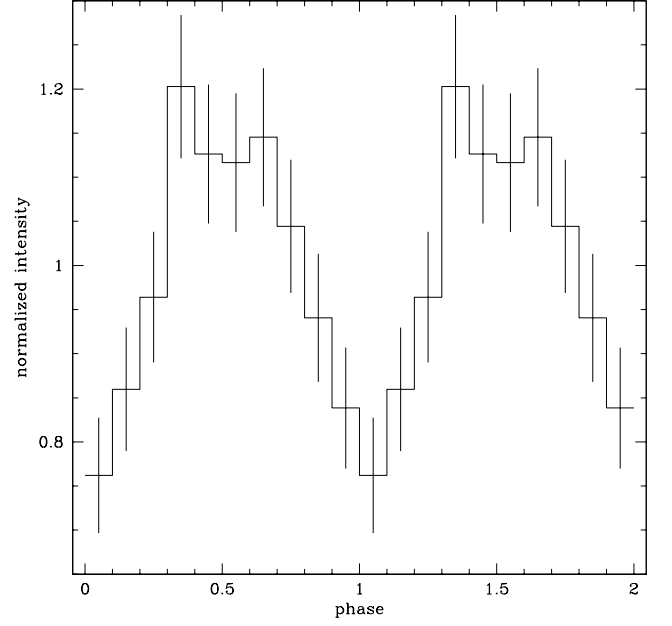
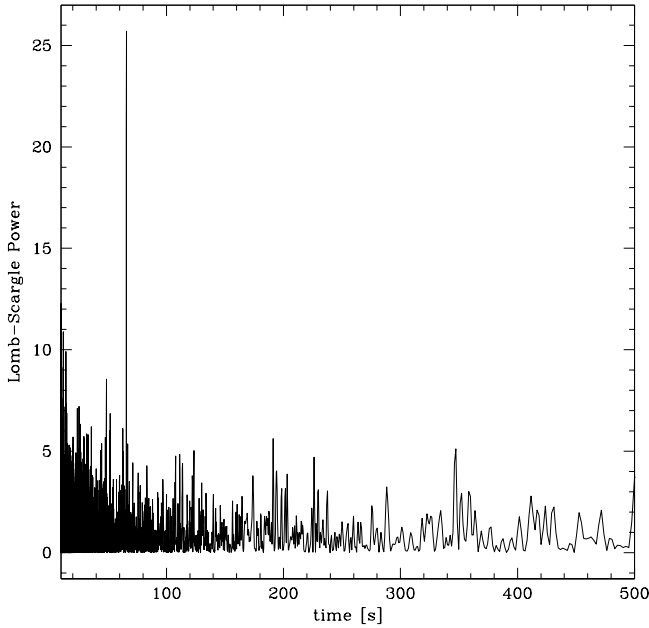
The 0.4–10 keV lightcurve is rather constant with a low average count rate of  $\sim 0.4$  counts s<sup>−1</sup>. No flare is observed. Considering the orbital period and duration of outbursts derived from the *INTEGRAL* long-term lightcurve, the expected outburst near the *XMM-Newton* observation happens between MJD 54188–54206. Therefore, *XMM-Newton* observed AX J1749.1–2733 at the beginning of one of its outburst (MJD 54190). The low EPIC/pn count rate is of the same order as the one observed with *INTEGRAL* during the large mosaics.

We searched for the pulsation computing the power density spectrum of both lightcurves. We used the fast computing method of the Lomb-Scargle periodogram proposed by Press & Rybicki (1989). The uncertainty of the period is computed using Eq. 14 of Horne & Baliunas (1986). Both periodograms are shown in Fig. 5 (*left column*). The maximum power is detected at  $66.09 \pm 0.07$  s and  $65.789 \pm 0.009$  s for pn and ISGRI, respectively. The corresponding folded lightcurves are also shown in Fig. 5 (*right column*) with zero epochs T0 of MJD 54190.391 and 52891.4, respectively. The pulse fractions, defined as  $P_f = (I_{\max} - I_{\min}) / (I_{\max} + I_{\min})$  with  $I_{\max}$  and  $I_{\min}$  being the maximum and minimum of the intensities of the folded lightcurve, reach  $22 \pm 6$  and  $29 \pm 11\%$ , respectively. The pulse profiles show one broad peak for pn and a slightly narrower one for ISGRI.

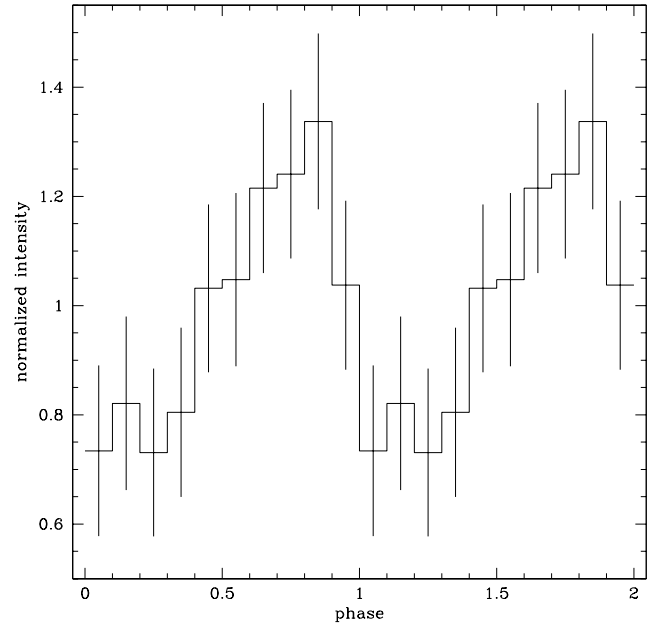
A pulsation of 132 s was reported by Karasev et al. (2007) using the same *XMM-Newton* data presented here and also the ISGRI data corresponding to the bright flare detected by *INTEGRAL*. No significant power appears at  $\sim 132$  s in both cases. In the pn periodogram, the closest stronger signals appear at 123 and 139 s, still their power are twice lower than the one at 66 s and they do not appear in the ISGRI periodogram. Folding the lightcurve at twice the period we derive show a double-peak



(a) EPIC/pn periodogram

(b) pn folded lightcurve,  $P = 66.09 \pm 0.07$  s and  $T_0 = \text{MJD } 54190.391$ 

(c) ISGRI periodogram

(d) ISGRI folded light curve,  $P = 65.789 \pm 0.009$  s and  $T_0 = \text{MJD } 52891.4$ 

**Fig. 5.** Periodograms and folded light curve for EPIC/pn (*top*, 0.4–10 keV) and ISGRI (*bottom*, 22–50 keV). The maximum power corresponds to  $66.09 \pm 0.07$  s and  $65.789 \pm 0.009$  s, respectively. The folded lightcurves use the derived periods and zero epochs of MJD 54190.391 and 52891.4, respectively.

profile in both folded lightcurves. Still, both local peaks show similar shape and intensity. The pulsation around 66 s is likely to be the real pulsation while the 132 s one is its first harmonic.

### 3.3. Spectral analysis

The broad-band *XMM-Newton*–*INTEGRAL* X-ray spectrum is shown in Fig. 6. The X-ray spectrum extracted with pn is combined with the hard X-ray one extracted during the bright flare seen in ISGRI. Therefore, an important constant factor must be applied as the intensity difference of AX J1749.1–2733 between the 2 observations is large. Still, the combined spectrum will

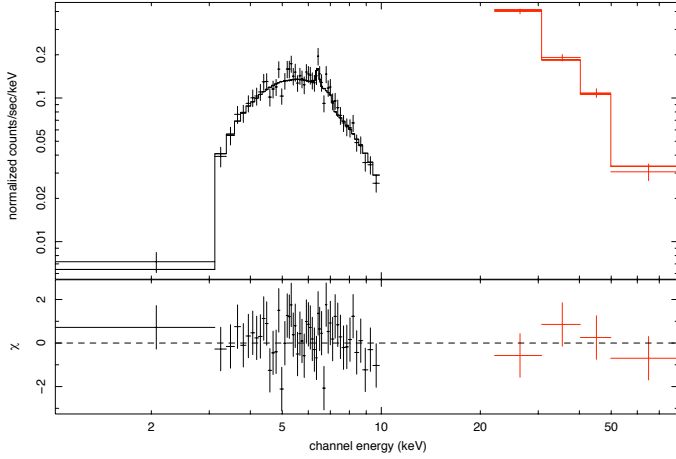


**Fig. 6.** High-energy broad-band spectrum of AX J1749.1–2733, combining the EPIC/pn and IBIS/ISGRI spectra. The best-fit model (absorbed PL with high-energy cutoff and an additional emission line) and residuals are also shown.

**Table 3.** Best fitting results for the broad-band spectrum. The model is `cons*wabs(cutoffpl+gaussian)`. The unabsorbed flux is computed setting  $N_H = 0$ .

Parameters	Values	Unit
$N_H$	$20.1^{+1.5}_{-1.3}$	$10^{22} \text{ H cm}^{-2}$
$\Gamma$	$1.0^{+0.1}_{-0.3}$	
$E_{\text{cut}}$	$21^{+5}_{-3}$	keV
$E_{\text{line}}$	$6.41^{+0.08}_{-0.07}$	keV
$F_{\text{line}}$	$1.3 \pm 0.9$	$10^{-5} \text{ ph cm}^{-2} \text{ s}^{-1}$
$EW_{\text{line}}$	52.5	eV
$C_{\text{ISGRI}}$	18	
$\chi^2_{\nu}$ (dof)	0.99 (103)	
unabs. 2–10 keV Flux	0.2	$10^{-10} \text{ ergs cm}^{-2} \text{ s}^{-1}$
unabs. 22–50 keV Flux	3.2	$10^{-10} \text{ ergs cm}^{-2} \text{ s}^{-1}$
unabs. 0.2–100 keV Flux	6.9	$10^{-10} \text{ ergs cm}^{-2} \text{ s}^{-1}$

constrain the spectral model that will fit the continuum shape of the source. The X-ray spectral bins are grouped to possess at least 30 counts per channel, allowing the usage of the  $\chi^2$  statistic.

First, the spectrum shows a strong absorption at low energies. Simple phenomenological models such as absorbed black body (BB) or power law (PL) fail to fit the data with  $\chi^2_{\nu}=3.4$  or 1.7 (each 106 d.o.f.), respectively. Disregarding the BB model, the absorbed PL clearly needs a high-energy cutoff to fit the data. The fit strongly improves with  $\chi^2_{\nu}=1.03$  (105 d.o.f.). We also explore the possibility of a line at 6.4 keV where some excess is visible. Again, the fit is slightly improved with  $\chi^2_{\nu}=0.99$  (103 d.o.f.). The possibility of an excess at low energies in addition to the absorption is also studied. However, the addition of a component at low energies is not significant as shown by the rather important value of the F-test probability of 0.1. The best fit parameters are listed in Table 3.

### 3.4. Identifying the optical/NIR counterpart

The field around AX J1749.1–2733 is very crowded, so it possesses several counterpart candidates within the error boxes of the previously reported high-energy missions. In Fig. 7, we show the field in the *J* band. With the higher accuracy of *Swift*, 3 2MASS candidates were reported (Romano et al. 2007). Still,

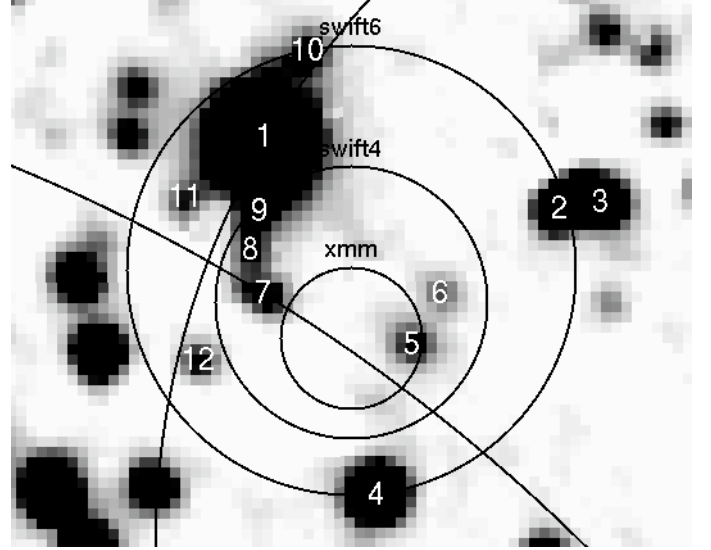


**Fig. 7.** SOFI image in filter *J*. The 12 candidates within the large *Swift* error box ( $6''$ ) are reported. Only the candidate #5 lies within the accurate X-ray position of *XMM-Newton* ( $2''$ ).

with SOFI, we note that there are 11 candidates in the *J* band within this  $6''$  *Swift* box<sup>10</sup>. With the improved *Swift* position given by Kong (2007), the 3 2MASS counterparts are ruled out, but 5 faint candidates remain. Taking into account the best X-ray position given by *XMM-Newton* (see Sect. 3.1), only candidate #5 remains as possible optical/NIR counterpart of AX J1749.1–2733. The source is not detected in filters *U*, *B* and *V*, but a faint source is detected in the other filters as highlighted in Fig. 8. The photometry of all sources is reported in Table 4.

## 4. Discussion and conclusion

The source possesses a long orbital period of  $185.5 \pm 1.1$  d and a spin period of  $\sim 66$  s. At the likely periastron passage, the source goes through an outburst whose duration is estimated to  $\sim 12$  d (with an upper-limit of  $\lesssim 18$  d). With such orbital period and outburst duration, the source is bright  $< 10\%$  of its time. The recurrence of such long outbursts related to the binary motion corresponds to type I outbursts observed in other BeHMXB (Coe 2000; Negueruela 2007). Furthermore, combining the observed pulsation and orbital period, AX J1749.1–2733 falls well in the BeHMXB arm of the Corbet diagram (*i.e.*  $P_{\text{spin}}$  vs  $P_{\text{orb}}$ ; Corbet 1984, 1986) strengthening its identification as a BeHMXB. The large orbital period rules out the possibility to associate this source with a low-mass X-ray binary.

A spin down of AX J1749.1–2733 is observed between the 2 observations of the bright flare with *INTEGRAL* and the *XMM-Newton* observation. We derive a spin down of  $\dot{P} = 0.08 \pm 0.02 \text{ s yr}^{-1}$  (*i.e.*  $\dot{\nu} = (-6.2 \pm 1.4) \times 10^{-13} \text{ Hz s}^{-1}$ ). Such spin down episodes have already been observed in other accreting pulsars, some examples being EXO 2030+375 with  $\dot{\nu} = -3.4 \times 10^{-14} \text{ Hz s}^{-1}$  and A0535+26 with  $\dot{\nu} = -2.2 \times 10^{-13} \text{ Hz s}^{-1}$  (Bildsten et al. 1997, and references therein). In order to have accretion onto a NS, the magnetic radius  $R_{\text{mag}}$  must be lower than the co-rotation radius  $R_{\text{cor}}$ . Otherwise, the infalling matter is centrifugally expelled by the magnetic field (that is the propeller regime, Illarionov & Sunyaev 1975). For a NS ( $M =$

<sup>10</sup> The 3 2MASS candidates correspond to sources #1, #4 and a blended source constituted of #2 and #3.

**Table 4.** Optical and NIR photometry of the candidate counterparts that are located within the large *Swift* error box. The candidate numbers correspond to those shown in Fig. 7. Only candidate #5 is located in the *XMM-Newton* error box. At the bottom, we show the parameters for the photometric solutions: *AM* the airmass, *Z<sub>p</sub>* the zero-point and *ext* the extinction.

Candidate	<i>R</i>	<i>I</i>	<i>J</i>	<i>H</i>	<i>K<sub>s</sub></i>
#1	22.6 ± 0.5	19.68 ± 0.04	12.485 ± 0.007	10.536 ± 0.009	9.178 ± 0.010
#2	–	–	16.32 ± 0.06	14.62 ± 0.04	13.51 ± 0.04
#3	–	–	15.84 ± 0.04	14.23 ± 0.03	13.27 ± 0.05
#4	–	–	15.27 ± 0.01	13.54 ± 0.01	12.45 ± 0.02
#5	21.3 ± 0.1	20.30 ± 0.09	17.42 ± 0.03	16.71 ± 0.02	15.75 ± 0.07
#6	–	–	18.08 ± 0.03	17.49 ± 0.05	16.1 ± 0.1
#7	20.15 ± 0.05	19.09 ± 0.03	17.33 ± 0.05	17.8 ± 0.4	–
#8	–	–	17.88 ± 0.09	17.4 ± 0.3	15.6 ± 0.1
#9	–	–	17.43 ± 0.06	15.97 ± 0.09	14.5 ± 0.2
#10	–	20.48 ± 0.09	17.23 ± 0.04	–	–
#11	–	–	18.11 ± 0.07	17.5 ± 0.2	16.0 ± 0.1
#12	–	20.7 ± 0.1	17.84 ± 0.07	18.2 ± 0.2	–
<i>AM</i>	1.054	1.052	1.150	1.114	1.076
<i>Z<sub>p</sub></i>	−0.44 ± 0.01	0.39 ± 0.01	1.84 ± 0.02	2.01 ± 0.02	2.6 ± 0.02
<i>ext</i>	0.091	0.051	0.13 ± 0.02	0.10 ± 0.02	0.07 ± 0.02

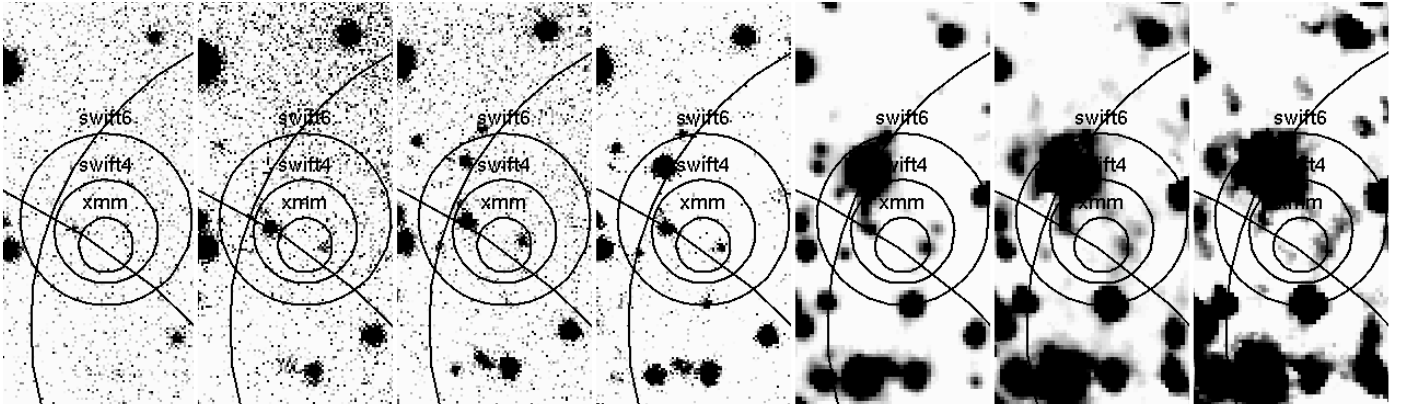


**Fig. 8.** Left to right: images in filters: *V*, *R*, *I*, *Z*, *J*, *H* and *K<sub>s</sub>*. The only candidate counterpart is visible from filters *R* to *K<sub>s</sub>*.

1.4  $M_{\odot}$ ,  $R = 10$  km) with a spin of 66 s, at the equilibrium point  $R_{\text{mag}} = R_{\text{cor}}$ , one estimates the magnetic field to be  $B = 6.5 \times 10^{12} \text{ G} \times (\dot{M}/10^{-10} M_{\odot} \text{ yr}^{-1})^{1/2}$ . The magnetic radius depends on the accreted matter flow as  $R_{\text{mag}} \propto \dot{M}^{-2/7}$ . Thus, the magnetic radius may exceed the co-rotation radius if the accretion rate becomes small enough, stopping the accretion. The infalling matter, expelled by propeller effect, can then remove some angular momentum, and decrease the spin period of the neutron star. With such large orbital period, the NS is in fact most of the time far from the dense accreting zone, where such effects leading to a decrease of the spin period can occur.

The broad X- and hard X-ray spectrum of AX J1749.1–2733 is similar to other HMXB pulsars (White et al. 1995). It is well fitted with an absorbed powerlaw and a high-energy cutoff with values  $N_{\text{H}} = 20.1^{+1.5}_{-1.3} \times 10^{22} \text{ cm}^{-2}$ ,  $\Gamma = 1.0^{+0.1}_{-0.3}$  and  $E_{\text{cut}} = 21^{+5}_{-3} \text{ keV}$ . The large absorption is in good agreement with the previous observation (*ASCA*, *Swift*; Sakano et al. 2002; Romano et al. 2007; Kong 2007), still it is largely better constrained with the EPIC/pn data. This large absorption is an order of magnitude higher than the galactic absorption expected in the line of sight of AX J1749.1–2733,  $N_{\text{H}}(\text{HI}) = 1.7 \times 10^{22} \text{ cm}^{-2}$  (interpolated from the HI map of Dickey & Lockman 1990). Thus, the X-ray source is intrinsically absorbed. The combination of the EPIC/pn and IBIS/ISGRI spectra allow us to better constrain the continuum getting a harder spectrum with a  $\Gamma$  that decreases by a factor 2 in comparison with former estimations and the ne-

cessity of the high-energy cutoff. Moreover, the BB+PL model ( $KT = 0.7^{+0.3}_{-0.1} \text{ keV}$  and  $\Gamma = 2.5 \pm 0.2$ ) proposed in Sguera et al. (2006) to fit the 20–60 keV spectrum can be discarded. The presence of a line at  $6.41^{+0.08}_{-0.07} \text{ keV}$  is in good agreement with the cold Fe  $K\alpha$  line that has been detected in other pulsars (White et al. 1995).

Only one candidate counterpart is located within the most accurate X-ray position of *XMM-Newton* (see Sect. 3.1). Using the relation of Predehl & Schmitt (1995) that links the X-ray absorption and the optical extinction,  $N_{\text{H}} (\text{cm}^{-2})/A_{\text{V}} (\text{mag}) = 1.79 \times 10^{21}$ , the expected optical extinction  $A_{\text{V}}$  is 9.5 magn assuming the reported galactic  $N_{\text{H}} = 1.7 \times 10^{22} \text{ cm}^{-2}$ . Then, the NIR extinctions are estimated as  $A_{\text{J}} = 2.680$ ,  $A_{\text{H}} = 1.663$  and  $A_{\text{K}} = 1.064$  using  $A_{\text{J}}/A_{\text{V}} = 0.282$ ,  $A_{\text{H}}/A_{\text{V}} = 0.175$  and  $A_{\text{K}}/A_{\text{V}} = 0.112$  (Rieke & Lebofsky 1985). Assuming a distance of 8.5 kpc, we derive the absolute magnitude as  $M_{\text{abs}} = m_{\text{app}} - 5 \log(\text{distance}/10 \text{ pc}) - A_{\text{V}}$ . We obtain  $M_{\text{J}} = 0.09$ ,  $M_{\text{H}} = 0.39$  and  $M_{\text{K}} = -0.05^{11}$ , so the colour is  $(J - K)_0 = 0.14$ . Thus, in a colour-magnitude diagram (CMD), the candidate companion star of AX J1749.1–2733 falls near the zone of the main sequence stars with spectral type between B5 and B8–A0 (see Fig. 9). However, the position of the source in the CMD strongly depends on the absorption and the distance chosen. In Fig. 9, we also report other possibilities varying the column density from

<sup>11</sup> The  $K_{\text{s}}$  magnitude is transformed into the  $K$  magnitude using the relation  $K - K_{\text{s}} = -0.005(J - K)$  (SOFI user manual, p.7).

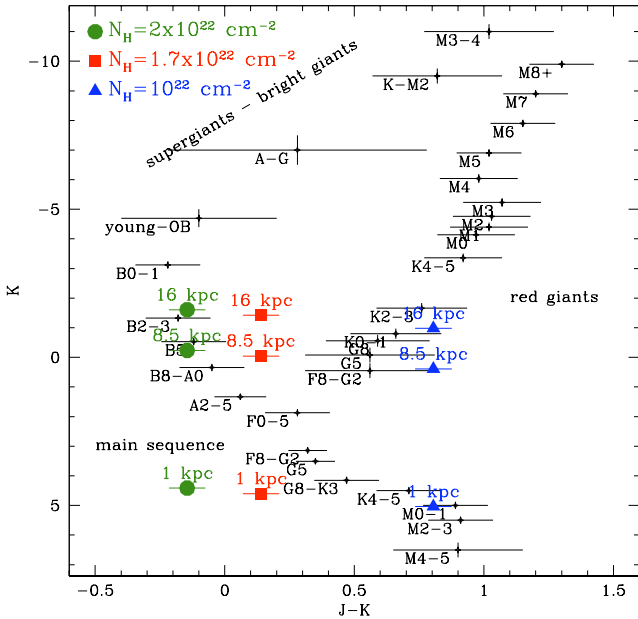


**Fig. 9.** Colour-magnitude diagram. The magnitudes here correspond to absolute magnitude. The location of the source #5 in the diagram is shown for several interstellar density columns and distances.

$1.0$  to  $2.0 \times 10^{22} \text{ cm}^{-2}$  and 3 different distances of 1, 8.5 and 16 kpc. With a lower extinction and a distance of 1 kpc, the star would be a main sequence star of type M. In that case, this star would unlikely be the counterpart of AX J1749.1–2733. Moreover, as pointed out earlier, the large orbital period completely rules out the possibility to combine such M star with this X-ray source. The possibility that the star is a red giant is also unlikely as it should combine a location far in the Galaxy with a low extinction. Spectroscopy of the candidate counterpart is needed to disentangle between the 2 possibilities, either a B star located far in the Galaxy  $\gtrsim 8.5$  kpc and strongly absorbed or a normal star located nearer to us. Still, because of the X-ray properties observed for AX J1749.1–2733 and the no presence of any other candidate, the B star is favoured. As the known BeHMXB have spectral type earlier than B3 (Negueruela 1998), this would imply that the source is located at a very high distance of  $> 8.5$  kpc. Assuming a distance of 8.5 kpc, the 22–50 keV luminosity is  $3 \times 10^{36} \text{ ergs s}^{-1}$  during the bright flare occurred at MJD 52891 and  $0.4 - 0.9 \times 10^{36} \text{ ergs s}^{-1}$  during the long outbursts, typical of BeHMXB flares. The 0.2–10 keV luminosity is  $0.2 \times 10^{36} \text{ ergs s}^{-1}$ , a factor 2–4 lower than in *INTEGRAL*. We point out that in the case of a BeHMXB with typical outbursts of the order of  $\sim 10^{36} \text{ ergs s}^{-1}$ , if the system was located nearer to us  $\leq 8$  kpc, *INTEGRAL* would detect such a source with a 22–50 keV count rate  $\gtrsim 2 \text{ counts s}^{-1}$  which is not the case.

In the case of a BeHMXB, AX J1749.1–2733 shows a high intrinsic absorption of  $N_{\text{H}} = 20.1^{+1.5}_{-1.3} \times 10^{22} \text{ cm}^{-2}$  that is quite uncommon in other BeHMXB. Indeed, most of the BeHMXB have density columns closer to the galactic absorption with  $N_{\text{H}} \sim 1 - 3 \times N_{\text{H}}^{\text{Gal}}$  (see Fig. 15 of Bodaghee et al. 2007). Only one BeHMXB exhibits such a high absorption: 2S 1845–024. The properties of this source are very similar to AX J1749.1–2733 with  $P_{\text{orb}} = 242.18 \pm 0.01 \text{ d}$ , outburst duration of  $\sim 13 \text{ d}$ ,  $P_{\text{spin}} = 94.9 \text{ s}$  (with episodes of spin-up and spin-down) and

$N_{\text{H}} = 25 \pm 10 \times 10^{22} \text{ cm}^{-2}$  (Koyama et al. 1990; Soffitta et al. 1998; Finger et al. 1999, and references therein). They classified 2S 1845–024 as a BeHMXB (located at 10 kpc<sup>12</sup>) from its X-ray properties, however no counterpart has been identified yet. Thus, AX J1749.1–2733 might be the first identified counterpart BeHMXB with a high intrinsic absorption similar to the obscured sgHMXB revealed by *INTEGRAL*. Spectral properties of pulsars, either sgHMXB or BeHMXB, are very similar (see e.g. White et al. 1995). As IBIS/ISGRI is not affected by absorption, *INTEGRAL* allowed to reveal a large population of obscured sgHMXB with  $N_{\text{H}}$  values of  $\gtrsim 10^{23} \text{ cm}^{-2}$ . The fact that such highly-absorbed BeHMXB have not been observed yet (Bodaghee et al. 2007) is perhaps not so surprising since BeHMXB are mostly transient sources and the sources must also be observed during the outbursts by another X-ray emission with high sensitivity at low energies (such as *XMM-Newton* or *Chandra*) in order to constrain the absorption. Such population of obscured BeHMXB might be still to be revealed. Indeed, the only BeHMXB among the *INTEGRAL* sources reported in Fig. 15 of Bodaghee et al. (2007) is the 3rd highly-absorbed BeHMXB (after AX J1749.1–2733 and 2S 1845–024).

All the X-ray properties observed in AX J1749.1–2733 lead to classify this object as an X-ray binary, most probably a HMXB with a Be companion star and whose compact object is a NS. The only optical/NIR candidate counterpart located inside the best X-ray error box is compatible with a B star located far in the galaxy and suffering large extinction. Besides, the lack of a supergiant companion and the duration/smoothness of the outbursts rule out the classification of this source as a SFXT as proposed in in’t Zand (2005) and Sguera et al. (2006). Instead, AX J1749.1–2733 seems to be an obscured BeHMXB located far away in the Galaxy.

**Acknowledgements.** The authors warmly thank the *XMM-Newton* team to accept the ToO request. SC thanks the ESO staff and especially Valenti Ivanov for performing the ToO observations. We also thank Jérôme Rodriguez for a careful re-reading of the manuscript and for giving useful comments. We would like to thank A. Lutovinov for discussing the nature of this source at the 5th *INTEGRAL* Anniversary workshop.

## References

- Arnaud, K. A. 1996, in *Astronomical Society of the Pacific Conference Series*, Vol. 101, *Astronomical Data Analysis Software and Systems V*, ed. G. H. Jacoby & J. Barnes, 17–+
- Bildsten, L., Chakrabarty, D., Chiu, J., et al. 1997, *ApJS*, 113, 367
- Bird, A. J., Malizia, A., Bazzano, A., et al. 2006, *ArXiv Astrophysics e-prints*
- Bodaghee, A., Courvoisier, T. J.-L., Rodriguez, J., et al. 2007, *A&A*, 467, 585
- Bodaghee, A., Walter, R., Zurita Heras, J. A., et al. 2006, *A&A*, 447, 1027
- Chaty, S., Rahoui, F., Foellmi, C., et al. 2008, *A&A* submitted
- Coe, M. J. 2000, in *Astronomical Society of the Pacific Conference Series*, Vol. 214, *IAU Colloq. 175: The Be Phenomenon in Early-Type Stars*, ed. M. A. Smith, H. F. Henrichs, & J. Fabregat, 656–+
- Corbet, R. H. D. 1984, *A&A*, 141, 91
- Corbet, R. H. D. 1986, *MNRAS*, 220, 1047
- Courvoisier, T. J.-L., Walter, R., Beckmann, V., et al. 2003, *A&A*, 411, L53
- Dean, A. J., Bazzano, A., Hill, A. B., et al. 2005, *A&A*, 443, 485
- Dickey, J. M. & Lockman, F. J. 1990, *ARA&A*, 28, 215
- Filliatre, P. & Chaty, S. 2004, *ApJ*, 616, 469
- Finger, M. H., Bildsten, L., Chakrabarty, D., et al. 1999, *ApJ*, 517, 449
- Götz, D., Falanga, M., Senziani, F., et al. 2007, *ApJ*, 655, L101
- Gros, A., Goldwurm, A., Cadolle-Bel, M., et al. 2003, *A&A*, 411, L179
- Horne, J. H. & Baliunas, S. L. 1986, *ApJ*, 302, 757
- Illarionov, A. F. & Sunyaev, R. A. 1975, *A&A*, 39, 185
- in’t Zand, J. J. M. 2005, *A&A*, 441, L1
- Jansen, F., Lumb, D., Altieri, B., et al. 2001, *A&A*, 365, L1

<sup>12</sup> This value can be considered as an upper limit as they derive it taking the minimum observed  $N_{\text{H}}$  as interstellar absorption without taking into account the intrinsic absorption.

- Karasev, D., Tsygankov, S., Lutovinov, A., Churazov, E., & Sunyaev, R. 2007, *The Astronomer's Telegram*, 1245, 1
- Kong, A. K. H. 2007, *The Astronomer's Telegram*, 1039, 1
- Koyama, K., Kunieda, H., Takeuchi, Y., & Tawara, Y. 1990, *PASJ*, 42, L59
- Kuulkers, E., Shaw, S. E., Paizis, A., et al. 2007, *A&A*, 466, 595
- Landolt, A. U. 1992, *AJ*, 104, 340
- Lebrun, F., Leray, J. P., Lavocat, P., et al. 2003, *A&A*, 411, L141
- Leyder, J.-C., Walter, R., Lazos, M., Masetti, N., & Produit, N. 2007, *A&A*, 465, L35
- Liu, Q. Z., van Paradijs, J., & van den Heuvel, E. P. J. 2000, *A&AS*, 147, 25
- Liu, Q. Z., van Paradijs, J., & van den Heuvel, E. P. J. 2006, *A&A*, 455, 1165
- Lutovinov, A., Revnivtsev, M., Gilfanov, M., et al. 2005, *A&A*, 444, 821
- Negueruela, I. 1998, *A&A*, 338, 505
- Negueruela, I. 2007, in *Astronomical Society of the Pacific Conference Series*, Vol. 367, *Massive Stars in Interactive Binaries*, ed. N. St.-Louis & A. F. J. Moffat, 477–+
- Negueruela, I., Smith, D. M., Reig, P., Chaty, S., & Torrejón, J. M. 2006, in *ESA SP-604: The X-ray Universe 2005*, ed. A. Wilson, 165–170
- Pellizza, L. J., Chaty, S., & Negueruela, I. 2006, *A&A*, 455, 653
- Persson, S. E., Murphy, D. C., Krzeminski, W., Roth, M., & Rieke, M. J. 1998, *AJ*, 116, 2475
- Predehl, P. & Schmitt, J. H. M. M. 1995, *A&A*, 293, 889
- Press, W. H. & Rybicki, G. B. 1989, *ApJ*, 338, 277
- Psaltis, D. 2006, *Accreting neutron stars and black holes: a decade of discoveries* (*Compact stellar X-ray sources*), 1–38
- Rieke, G. H. & Lebofsky, M. J. 1985, *ApJ*, 288, 618
- Rodríguez, J., Bodaghee, A., Kaaret, P., et al. 2006, *MNRAS*, 366, 274
- Romano, P., Mangano, V., Cucchiara, A., & Sidoli, L. 2007, *The Astronomer's Telegram*, 1040, 1
- Sakano, M., Koyama, K., Murakami, H., Maeda, Y., & Yamauchi, S. 2002, *ApJS*, 138, 19
- Sguera, V., Bazzano, A., Bird, A. J., et al. 2006, *ApJ*, 646, 452
- Smith, D. M., Heindl, W. A., Markwardt, C. B., et al. 2006, *ApJ*, 638, 974
- Soffitta, P., Tomsick, J. A., Harmon, B. A., et al. 1998, *ApJ*, 494, L203+
- Strüder, L., Briel, U., Dennerl, K., et al. 2001, *A&A*, 365, L18
- Turner, M. J. L., Abbey, A., Arnaud, M., et al. 2001, *A&A*, 365, L27
- Ubertini, P., Lebrun, F., Di Cocco, G., et al. 2003, *A&A*, 411, L131
- Walter, R., Rodríguez, J., Foschini, L., et al. 2003, *A&A*, 411, L427
- Walter, R., Zurita Heras, J., Bassani, L., et al. 2006, *A&A*, 453, 133
- White, N. E., Nagase, F., & Parmar, A. N. 1995, *X-ray binaries* (*Cambridge Astrophysics Series*, Cambridge, MA: Cambridge University Press, —c1995, edited by Lewin, Walter H.G.; Van Paradijs, Jan; Van den Heuvel, Edward P.J.), 1–57
- Winkler, C., Courvoisier, T. J.-L., Di Cocco, G., et al. 2003, *A&A*, 411, L1
- Zurita Heras, J. A., Chaty, S., & Rodríguez, J. 2007, *The Astronomer's Telegram*, 1035, 1
- Zurita Heras, J. A., de Cesare, G., Walter, R., et al. 2006, *A&A*, 448, 261